Contrasting the excited state reaction pathways of phenol and *para*-methylthiophenol in the gas and liquid phases†

Yuyuan Zhang,§‡[a] Thomas A. A. Oliver,§¶[b] Michael N. R. Ashfold[b] and Stephen E. Bradforth*[a]

Received 3rd March 2012, Accepted 23rd March 2012
DOI: 10.1039/c2fd20043k

To explore how the solvent influences primary aspects of bond breaking, the gas and solution phase photochemistries of phenol and of *para*-methylthiophenol are directly compared using, respectively, H (Rydberg) atom photofragment translation spectroscopy and femtosecond transient absorption spectroscopy. Approaches are demonstrated that allow explicit comparisons of the nascent product energy disposals and dissociation mechanisms in the two phases. It is found, at least for the case of the weakly perturbing cyclohexane environment, that most aspects of the primary reaction dynamics of the isolated molecule are reproduced in solution. Specifically, in the gas phase, both molecules can undergo fast X–H (X=O, S) bond dissociation upon excitation with short wavelengths ($193 < \lambda_{pump} < 216$ nm), following population of the dissociative S_2 ($1^1\pi\sigma^*$) state. Product electronic branching, vibrational and translational energy disposals are determined. Photolysis of phenol and *para*-methylthiophenol in solution at 200 nm results in formation of vibrationally excited radicals on a timescale shorter than 200 fs. Excitation of *para*-methylthiophenol at 267 nm reaches close to the S_1 ($1^1\pi\pi^*$)/S_2 ($1^1\pi\sigma^*$) conical intersection (CI): ultrafast dissociation is observed in both the isolated and solution systems—again indicating direct dissociation on the S_2 potential energy surface. Comparing results for this precursor at different excitation energies, the extent of geminate recombination and the derived H-atom ejection lengths in the condensed phase photolyses are in qualitative agreement with the translational energy release measured in the gas phase studies. Conversely, excitation of phenol at 267 nm prepares the system in its S_1 state at an energy well below its S_1/S_2 CI; the slow O–H bond fission inferred in the gas phase experiments is observed directly in the time-resolved studies in cyclohexane solution *via* the appearance of phenoxyl radical absorption after ~1 ns, with only S_1 excited state absorption discernible at earlier delay times. The slow O–H bond fission in solution provides additional evidence for a tunnelling dissociation mechanism, where the H atom tunnels beneath the lower diabats of the S_2/S_1 CI. Finally, the photodissociation of phenol clusters in solution is considered, where evidence is presented that the O–H dissociation coordinate is impeded in H-bonded dimers.

[a]*Department of Chemistry, University of Southern California, Los Angeles, CA 90089, USA. E-mail: stephen.bradforth@usc.edu; Fax: (+213) 740-3972; Tel: (+213) 740-0461*
[b]*School of Chemistry, Cantocks Close, University of Bristol, BS8 1TS, UK*

† Electronic supplementary information (ESI) available. See DOI: 10.1039/c2fd20043k
‡ Present address: Department of Chemistry and Biochemistry, Montana State University, Bozeman, Montana 59715, USA
§ These authors contributed equally to this work
¶ Present address: Department of Chemistry, University of California, Berkeley, CA 94720, USA

I. Introduction

Weakly interacting solvents, like rare gas matrices, are generally considered excellent mimics of a gas phase environment in terms of their effect on the shapes of molecular potential energy surfaces (PESs).[1] Thus exploring the photochemistry of solutes in inert solvents such as cyclohexane provides an instructive approach to see how dissociative reaction dynamics map into the condensed phase. However, such solvents still provide some dynamical complexities when compared to the collision-free environment. For example, collision between the nascent reaction products and the solvent molecules can alter the vibrational energy disposal, as solvent molecules provide an effective sink for vibrational energy relaxation (VER).[1–4] Similarly, the translational motion of products will be eventually stopped due to the friction exerted by the solvent.[5–7] Subsequent diffusion of the incompletely separated reaction products in the solvent can lead to geminate recombination.[3,8] Although interactions with solvent molecules have modest changes on the PES landscape, differential solvation of electronic states can lead to larger changes in the location of the conical intersections (CIs), and affect how the excited state molecules approach (*i.e.*, the velocity and the angle) and thus branch through CIs.[9]

In the collision-free, gas phase environment, the X–H (X=N, O, S) bond fission in heteroaromatic molecules has been determined to be an important non-radiative deactivation pathway following UV photoexcitation.[10] In such systems, the $^1\pi\sigma^*$ state is the PES responsible for X–H bond fission, as predicted by pioneering *ab initio* calculations[11] and demonstrated by gas phase photodissociation experiments such as H(Rydberg) Atom Photofragment Translational Spectroscopy (HRA-PTS)[10,12–15] and velocity map ion-imaging (VMI).[16,17] The $^1\pi\sigma^*$ state is formed initially by 3s $\leftarrow$ π electronic promotion (in the case that X=N, O) in the vertical Franck–Condon region. Upon X–H bond extension, the Rydberg 3s orbital evolves into the anti-bonding σ^* orbital localised across the X–H bond. For simplicity, we henceforth refer to such mixed Rydberg-valence dissociative states as $^1\pi\sigma^*$ states.

In the case of phenol (PhOH), the diabatic S_2 ($1^1\pi\sigma^*$) PES is repulsive with respect to the O–H bond extension and intersects with the diabatically bound S_1 ($1^1\pi\pi^*$) state to form the S_1 ($1^1\pi\pi^*$)/S_2 ($1^1\pi\sigma^*$) CI as displayed in Fig. 1(a). Previous HRA-PTS experiments clearly demonstrated two distinct time scales for H atom generation: slow, when PhOH is excited into vibrational levels of the S_1 state at energies below the S_1/S_2 CI, and fast when the $^1\pi\sigma^*$ state is populated directly which can occur for excitation with $\lambda_{pump} < 248$ nm.[13,18–20]

The highest occupied molecular orbital (HOMO) of phenol is largely comprised of the benzene π orbital with some contribution from the oxygen $2p_x$ lone pair as shown in Fig. 1(a) whereas, in thiophenol (formed by substituting the O atom in phenol with an S atom), the S $3p_x$ lone pair makes a much greater contribution. Further, as Fig. 1(b) shows, the S_2 potential energy curve (PEC) in *para*-methylthiophenol (*p*-MePhSH) shows negligible evidence of a "shelf" in the vertical Franck–Condon (vFC) region (*cf.* phenol in Fig. 1(a)), presumably reflecting the much reduced overlap of the 4s and σ^* orbitals.[21] Fig. 1(b) also shows that the dissociative S_2 and diabatically bound S_1 PECs of *p*-MePhSH intersect, but the resulting CI is very close to the S_1 potential minimum, enabling prompt formation of *para*-methylthiophenoxyl (*p*-MePhS) and H atom products even when exciting at the S_1 "origin" ($\lambda_{pump} = 295$ nm).[21,22] This is evident from the HRA-PTS experiments, which show that the H atoms generated by $\lambda_{pump} \leq 295$ nm have an anisotropic recoil velocity distribution, implying that S–H bond fission occurs on a time scale that is shorter than the parent rotational period.[21,22] Further, and in contrast to PhOH, S–H bond fission on the $1^1\pi\sigma^*$ PES yields a significant yield of both *p*-MePhS($\tilde{X}^2B_1$) and *p*-MePhS($\tilde{A}^2B_2$) radical products, as a result of branching at the S_2/S_0 ($1^1\pi\sigma^*/S_0$) CI. Branching for this family of molecules, but not in PhOH, has been rationalised by Landau–Zener arguments;[14,21,23] the energy difference between the ground and excited radical is much smaller in the case of *p*-MePhS and the CI occurs

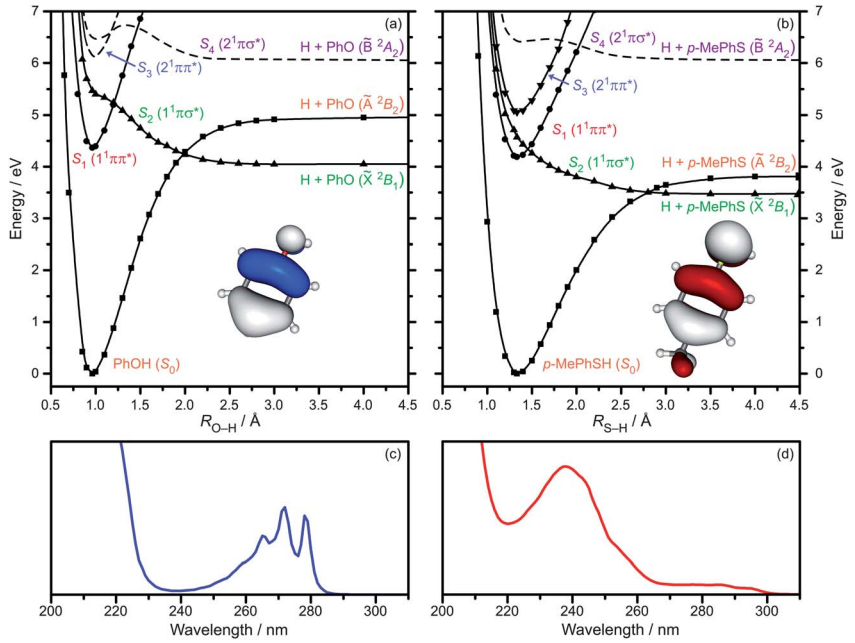

Fig. 1 (a) Optimized PECs along R_{O-H} for PhOH, calculated at the CASPT2(10/10)/aug(O)-AVTZ level for the ground state (S_0), S_1 ($1^1\pi\pi^*$) and S_2 ($1^1\pi\sigma^*$) excited states (reproduced from ref. 19); (b) CASPT2(10/10)/aug(S)-cc-pVTZ PECs in R_{S-H} for *p*-MePhSH for the same electronic states as in (a) plus the S_3 ($2^1\pi\pi^*$) state.[77] The dashed curves in (a) and (b) depict our best estimate of the minimum energy pathway along the given states, based on prior experimental and theoretical studies. The HOMO for each molecule is displayed in the lower right hand corner of each panel. UV electronic absorption spectra of (c) PhOH and (d) *p*-MePhSH in cyclohexane were taken at room temperature.

at noticeably longer R_{X-H} bond distances (see Fig. 1). Out-of-plane (a'') modes facilitate the transfer of flux between the S_2 ($^1A''$) and S_0 ($^1A'$) PECs and thus modulate the $\tilde{A}/\tilde{X}$ state radical branching. The *p*-MePhS products carry excitation in ring breathing and C–S wagging modes—reminiscent of the vibrational energy disposal in the PhO products from photolysis of PhOH—but the majority of the excess energy is partitioned into H atom translational excitation, especially when exciting at λ_{pump} <~266 nm.[21]

We have previously studied the photodissociation of *p*-MePhSH in the gas phase and in one solvent, liquid ethanol.[21,22] S–H bond fission motifs characteristic of the gas phase dynamics were found to transfer to the condensed phase, and no evidence was found for other competing pathways unique to the condensed phase, such as photoionisation, excited state proton transfer or proton-coupled electron transfer. From our femtosecond transient absorption (TA) experiments, dissociation in ethanol solution was established to occur within the instrument response time (~50 fs). *p*-MePhS($\tilde{X}$) radical is clearly discernable as a result of this ultrafast dissociation, but we cannot rule out the generation of *p*-MePhS($\tilde{A}$) radicals.[22] The formation of an adduct was also discerned on longer timescales, and assigned to a diffusive re-encounter of the primary H atom attacking the ring of the *p*-MePhS radical,[22,24] its geminate partner from the initial photodissociation event.

The current study aims to investigate a broader range of energy disposals, varying the solute (PhOH *vs.* *p*-MePhSH), the photolysis wavelength (and thus different X–H bond fission pathways) and the environment (isolated gas phase *vs.* solution). In this way, we can further explore similarities and differences in the gas and solution photochemistry. In this report we will consider a solution environment, liquid

cyclohexane, in which solute–solvent interactions will be relatively weak and thus the gas phase PESs might reasonably be expected to apply, at least to first order. Although the PESs might be little changed, the solvent may influence the location of, and dynamic approach to, individual CIs. We will therefore explore to what extent the dynamic observables such as the translational recoil motion of the H atom, the energy disposal patterns into the various electronic and vibrational degrees of freedom in the radical fragments can be deduced, and then connected back to the gas phase behaviour. Cyclohexane also provides an environment where hydrogen-bonded solute dimers can be studied; we provide a first exploration of this topic by carrying out photolysis experiments on phenol clusters.

II. Experimental and theoretical methods

The HRA-PTS experiment at Bristol has been described previously.[13,18,21,22] *p*-MePhSH (Sigma Aldrich, 98%) and PhOH (Fluka, 99.5%) are solids at room temperature and were placed in an inline filter and resistively heated to 70 and 50 °C, respectively, in order to generate sufficient vapour pressure. The resulting vapour pressures were each seeded in ~700 Torr of Ar and pulsed through a solenoid valve creating a supersonic beam. This was subsequently skimmed and intersected by the frequency doubled output of a tuneable nanosecond pulsed laser ($266 \geq \lambda_{pump} \geq 206$ nm) or an ArF excimer laser ($\lambda_{pump} = 193$ nm). H atom photoproducts formed in the interaction region were double-resonantly excited after a time delay $\delta t \sim 10$ ns, *via* the 2p state by 121.6 nm (Lyman-α) radiation, and then to a high Rydberg state ($n \sim 80$) using a second ~366 nm photon. Any prompt ions formed within the interaction region were extracted using a biased deflector plate that straddles the interaction region. Rydberg-tagged H atoms that fly the known distance, d, to the detector are field ionized upon passing through a grounded mesh and detected. H atom time-of-flight (TOF) spectra are then converted into total kinetic energy release (TKER) spectra using eqn (1):

$$\mathrm{TKER} = \frac{1}{2} m_{\mathrm{H}} \left(1 + \frac{m_{\mathrm{H}}}{m_{\mathrm{R}}}\right) \left(\frac{d}{t}\right)^2 \quad (1)$$

where m_H is the mass of the hydrogen atom (1.00794 u), m_R is the mass of the assumed co-fragment, (*p*-MePhS = 123.20 u, PhO = 93.11 u), and t is the time taken for the H atoms to reach the detector. A t^{-3} Jacobian was applied when transforming the measured TOF signal intensities into TKER space.

The TA experiments at the University of Southern California were achieved by exciting the solution of interest with UV pulses ($\lambda_{pump} = 267$ and 200 nm) and probing the transient species with a broadband super continuum pulse (typically $310 \leq \lambda_{probe} \leq 650$ nm). To make ultrashort 267 nm, the 800 nm fundamental (1 kHz, Coherent Legend) was converted to deep ultraviolet by four-wave mixing (4WM) in an argon-filled hollow core fibre.[25] The resulting pulses centred at 267 nm had a bandwidth of 6 nm, and were subsequently compressed by a pair of Gires–Tournois Interferometer negative dispersion mirrors,[26] generating a 60 ± 10 fs (FWHM) pulse with very little higher order dispersion, as determined by pulse cross-correlation by two-photon absorption in ethanol. Photolysis was also carried out at 267 and 200 nm using longer pump pulses obtained by 3rd and 4th harmonic generation by sum-frequency mixing in a BBO crystal; these pulses had bandwidths of 2 nm and 1 nm and pulse widths of 100 fs and 130 fs, respectively, as determined by cross-correlation. All experiments employed pump fluences in the range $3.2 \leq F \leq 9.6$ mJ cm^{-2}. The transient signal of the solute was linearly dependent on the pump fluence, as determined by a power dependence study in which the 267 nm pump fluence was varied across the range $0.4 \leq F \leq 13.6$ mJ cm^{-2}. Alternate pump pulses were blocked by a chopper operating at 500 Hz. The weak super continuum probe was generated by focusing a small portion of the 800 nm

fundamental into a rotating CaF_2 disc. A pair of off-axis aluminium-coated parabolic mirrors was used to collimate and then focus the super continuum into the sample. The transmitted super continuum was dispersed onto a 256-pixel silicon diode array, where signals with and without the pump beam present were recorded to determine the transient absorption at a given time delay. The relative polarisation of the pump and probe radiation was controlled by rotating a zero-order half wave plate in the 800 nm beam driving the continuum generation. The temporal chirp of the continuum was corrected mathematically by setting the coherent pump + probe two-photon absorption peak from solvent alone at each probe wavelength to zero delay.[27] The sample was delivered by a wire guided gravity jet, forming a thin film of thickness 50–80 μm at the detection region. The flow rate of the liquid ensures that a fresh sample was interrogated every pump pulse.[28] For the TA experiments, various concentrations (10, 45 and 90 mM) of PhOH (99.5%, Avocado Research Chemicals) and *p*-MePhSH (97%, TCI America) were used in cyclohexane (>99.0%, HPLC and UV-Spectrophotometric grade, EMD or Mallinckrodt) without further purification.

Time-resolved emission from PhOH was obtained *via* time-correlated single photon counting (TCSPC), where phenol was excited at 267 nm and the decay of the fluorescence maximum (at 300 nm, determined by steady sate emission) was monitored. ~0.1 mM phenol solutions in cyclohexane were used to produce an optical density (O.D.) = ~0.1 in the 1 cm quartz cell.

The ground state geometries of PhOH and *p*-MePhSH were optimized with Møller–Plesset second order perturbation theory (MP2) and an aug-cc-pVTZ basis set. For the sulphur atom, an aug-cc-pV(T + *d*)Z basis was used for these and all subsequent calculations. To ensure the geometry optimization converged to a true minimum, the gradient convergence criteria were tightened to 1×10^{-6} a.u. Vertical excited state absorption (ESA) spectra for the S_1 states of PhOH and *p*-MePhSH were calculated using the equation of motion coupled cluster with single and double excitations (EOM-CCSD) methodology and an aug-cc-pVTZ basis set. Transition dipole moments (TDMs) for excitations from the S_1 state to higher excited singlet (S_n) states were calculated for both molecules for energies up to $E < 4.28$ eV (*i.e.*, $\lambda > \sim 290$ nm).[29]

Relaxed potential energy cuts (PECs) for PhOH in the O–H stretch coordinate, R_{O-H}, are reproduced from ref. 19. The corresponding PECs for *p*-MePhSH in the R_{S-H} coordinate were calculated in this study for the ground, $1^1\pi\pi^*$, $1^1\pi\sigma^*$ and $2^1\pi\pi^*$ states, which correspond to the diabatic S_0, S_1, S_2 and S_3 electronic states. These calculations were performed using complete active self consistent field (CASSCF) theory and a set of ten electrons in ten orbitals active space (10/10). The active space was comprised from the 3 benzene ring centred π, S–H σ and the S($3p_x$) conjugated lone pair occupied orbitals, three ring centred π*, the S–H anti-bonding σ* and S(4s) Rydberg virtual orbitals. The basis set described above was used, but with additional diffuse functions on the sulphur atom in order to allow for a better description of any Rydberg-valence mixing; henceforth this is termed the aug(S)-cc-pVTZ basis set. CASSCF calculations for each excited state were state-averaged with the S_0 wavefunction. At each given S–H bond extension, the geometry was allowed to relax on each PES, thus providing the minimum energy pathway or curve. Complete active space with second order perturbation theory (CASPT2) single point energies were then calculated at these optimized geometries, which required an imaginary level shift to avoid intruder state problems. All *ab initio* calculations were performed in Molpro.[30]

III. Results

i. Photolysis in the gas phase

Total kinetic energy release (TKER) spectra for the H + radical products from these photodissociation reactions obtained at many, particularly longer, photolysis

wavelengths have been reported in earlier publications.[13,18,21,22,31] These provide important information about the product energy release and branching in the "unperturbed" dissociation reaction. To aid comparison with the solution studies presented here, additional TKER spectra of the products from *p*-MePhSH and PhOH photolysis at wavelengths ~200 nm are displayed in Fig. 2(a) and (b), respectively. It is immediately observed that photolysis at $193 < \lambda_{pump} < 216$ nm yields broad, featureless TKER spectra, indicative of highly vibrationally excited photofragments in both cases. This should be compared with behaviour found at longer photolysis wavelengths, where vibrationally structured spectra are observed. In addition, the energy partitioned into H atom translation at ~200 nm is now substantially larger (up to 22 000 cm^{-1})—not unsurprisingly, given the much higher photoexcitation energies and the fact that most of the radical products are still formed in the same electronic states as at lower excitation energies.

Both $\tilde{X}$ and $\tilde{A}$ state *p*-MePhS radicals are observed in the photolysis of *p*-MePhSH.[21,22] These two states are separated by 3320 ± 50 cm^{-1} as shown in Fig. 1(a).[21,22] It is notable, however, that on reducing the photolysis wavelength from 216 nm to 193 nm, and thereby increasing the available energy by 5 500 cm^{-1}, very little of the additional energy appears as translation. Most of the additional energy is channelled into vibrational excitation of the nascent radical. $\tilde{X}$ state PhO products are dominant in the UV photolysis of phenol at all photolysis wavelengths so far studied, although evidence from 230 nm photolysis of phenol-d_5 suggests that some small fraction of the $\tilde{A}$ state radicals can be formed.[18] Comparing the $\lambda = 193$ nm dataset with $\lambda = 206$ nm in Fig. 2, an additional structured feature is observed centred at TKER ~5 000 cm^{-1}. This feature is attributable to the PhO($\tilde{B}$) radical.[18] Stavros and co-workers were unable to identify PhO($\tilde{B}$) radicals in an ultrafast VMI study of phenol photolysis at 200 nm[32] and suggested, consistent with the calculated PECs presented here (Fig. 1(b)) and in ref. 18, that the H + PhO($\tilde{B}$) product channel remains closed at $\lambda = 200$ nm. Again, reducing the photolysis wavelength from 206 to 193 nm increases the total available energy by 3 200 cm^{-1} but, as Fig. 2 shows, very little of this additional energy is released as H atom translational recoil.

Table 1 compares the average TKERs for both dissociation reactions in the gas phase at these short photolysis wavelengths with results at longer wavelengths. Most of the energy release at $\lambda = 266$ nm is partitioned into translation.

ii. Solution photodissociation of *p*-MePhSH

Fig. 3(a) displays representative TA spectra of *p*-MePhSH in cyclohexane solution following excitation with a 60 fs 267 nm pump pulse. Features attributable to

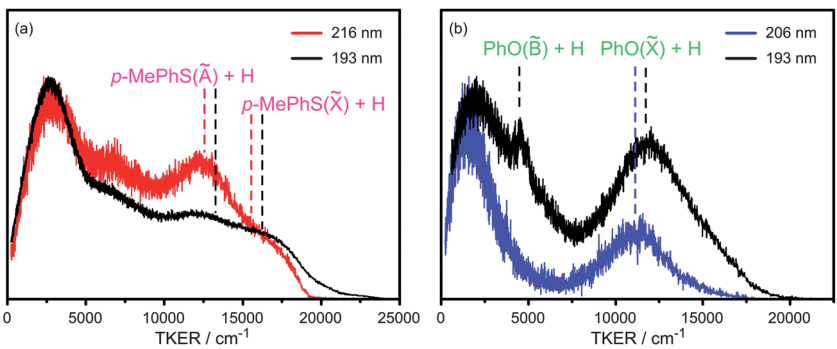

Fig. 2 TKER spectra derived from HRA-PTS studies of (a) *p*-MePhSH and (b) PhOH at photolysis wavelengths shown in legend. The combs above the datasets in each panel represent the estimated average TKER for the respective product channels as given in Table 1.

Table 1 Comparison of maximum possible ($TKER_{max}$) and average measured TKERs of products arising from excited state X–H bond fission in *p*-MePhSH and PhOH at selected photolysis wavelengths

λ_{phot}/nm	193	206	216	266
Excitation Energy/cm^{-1}	51 813	48 544	46 296	37 594
p-MePhSH[b]				
$TKER_{max}$ ($\tilde{X}$)/cm^{-1}	24 380	—	18 870	10 160
$TKER_{max}$ ($\tilde{A}$)/cm^{-1}	21 060	—	15 550	6 840
Average TKER($\tilde{X}$)/cm^{-1}	~16 500[c]	—	~16 000[d]	~10 000[c]
Average TKER($\tilde{A}$)/cm^{-1}	~13 200[c]	—	~12 700[d]	~6 700[c]
PhOH[a]				
$TKER_{max}$/cm^{-1}	21 800	18 530	—	7 580
Average TKER/cm^{-1}	~12 000[e]	~11 500[f]	—	~5 600[g]

[a] D_0(PhO–H) = 30015 ± 40 cm^{-1} from ref. 13. [b] D_0(*p*-MePhS–H) = 27430 ± 50 cm^{-1}, $\Delta E(\tilde{A} - \tilde{X})$ = 3320 ± 50 cm^{-1} from ref. 21, 22. [c] ref. 21, 22. [d] ref. 21. [e] ref. 18. [f] Current work. [g] Data for 275.1 nm, the S_1 origin from ref. 13. Unpublished data at 266 nm shows a negligible difference in the average TKER.

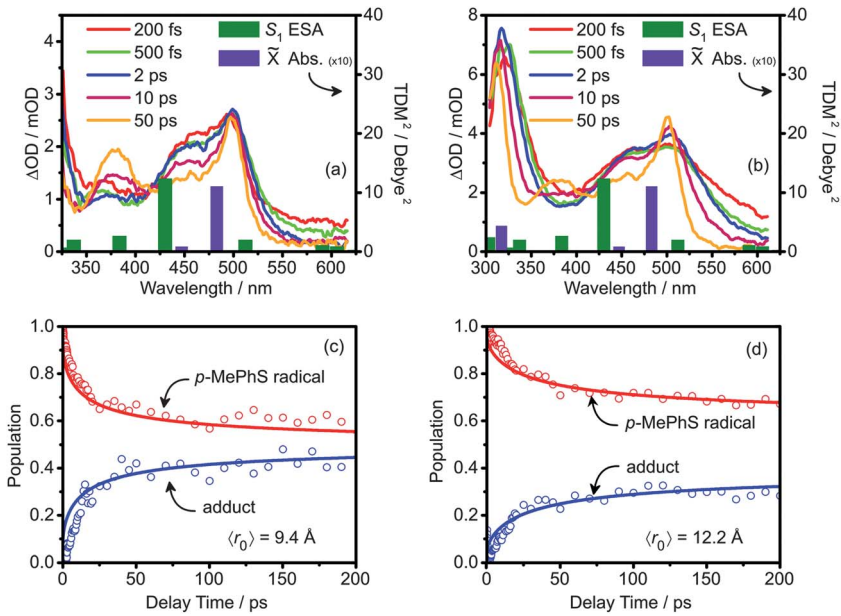

Fig. 3 (a) TA spectra measured at selected delay times following 267 nm photolysis of *p*-MePhSH in cyclohexane, with the pump–probe polarisation set to magic angle. (b) TA spectra measured following 200 nm photolysis of *p*-MePhSH in cyclohexane (magic angle polarisation). The squares of the calculated transition dipole moments (TDM^2) for transitions originating from S_1 (ESA) and from *p*-MePhS radicals are also shown (as bars in each panel). The radical transitions are from CASPT2/CASSCF calculations of ref. 22 and the S_1 band predictions are from the current EOM-CCSD calculations. (c, d) Geminate recombination analysis from the radical (red) and adduct (blue) kinetics after 267 nm and 200 nm photodissociation, respectively. The lines represent the survival probabilities, $\Omega(t)$, of the radical and the population rise of the adduct, as predicted by a radical–radical geminate recombination model and using physical constants described in ref. 22. From this analysis, the average ejection lengths $\langle r_0 \rangle$ are shown.

p-MePhS($\tilde{X}$) radicals, centred at λ_{probe} = 500, 450 and <320 nm,[22,33] are clearly evident within the overall instrument response time (~100 fs) and are consistent with prompt S–H bond dissociation. The band assignments and amplitudes are generally in accord with previously computed CASPT2 energies and CASSCF transition dipole moments for the gas phase radical (purple bars shown at base of Fig. 3).[22] The radical electronic absorption bands measured in cyclohexane at any given pump–probe time delay are sharper than in the equivalent TA spectrum in ethanol measured previously.[22,24] Such differences reflect the weaker solute–solvent interactions in the non-polar cyclohexane.[34,35]

Over longer time delays (t > 5 ps), the absorptions assigned to the *p*-MePhS($\tilde{X}$) radical decay and a transient centred at ~380 nm appears. The latter has previously been assigned to adduct formation.[22,24] The appearance kinetics of this feature, as well as the decay kinetics at 500 nm, are insensitive to the *p*-MePhSH concentration (data not shown)—consistent with a product formed from geminate recombination of the primary radical pair.

We have previously assigned the 450 nm shoulder to the *p*-MePhS($\tilde{C} \leftarrow \tilde{X}$) transition, which in the previous CASPT2(9/8)/aug-cc-pVTZ calculations, is predicted to have weak absorption strength, arguing that it gained intensity by vibronic mixing with the stronger $\tilde{B} \leftarrow \tilde{X}$ transition centred at ~500 nm.[22] In cyclohexane, unlike in ethanol, it is apparent that the 450 nm side of the band decays to about 50% of the height of the 500 nm band by ~50 ps. Thus, the different kinetics at the two marker wavelengths suggests that they cannot trace the same population and that another shorter lived species must contribute to the absorption measured at 450 nm. The new electronic structure calculations presented here are helpful in understanding this aspect of the spectral evolution. The EOM-CCSD/aug-cc-pVTZ calculations suggest a series of very bright transitions originating in the excited S_1 state within the broadband continuum range (green bars shown at base of figures), consistent with the idea of a "broad underlying absorption" assigned to S_1 ESA earlier,[22] but highlight an S_1 transition centred at ~430 nm with substantial TDM (green bars at base of Fig. 3). This transition is close to the 450 nm shoulder observed in our TA experiments, and it is likely therefore that the latter contains some contribution from S_1 ESA (in addition to *p*-MePhS($\tilde{C} \leftarrow \tilde{X}$) absorption)—thus explaining the complicated evolution of the spectrum in this region. The only part of the transient spectrum that perhaps can be assigned cleanly to parent ESA is at wavelengths ≥600 nm. Most of this signal decays rapidly (within 1 ps); signal to noise precludes assessing whether any small part of this absorption is long-lived (hundreds of picoseconds), as seen in our earlier studies in ethanol. The order-of-magnitude difference in the calculated TDMs for ESA compared to radical absorption suggest that little population is actually created or trapped on S_1 and its contribution appears 'exaggerated' by virtue of its much larger oscillator strength (*cf.* the *p*-MePhS radical absorptions).

Fig. 3(b) displays representative TA spectra when *p*-MePhSH is photoexcited at 200 nm. The spectral signatures for the *p*-MePhS($\tilde{X}$) radical at 425–500 nm are readily observed within the 180 fs instrument response time, again implying ultrafast S–H bond fission. The initial contour of this band is much broader than that observed at 267 nm excitation, as expected if the *p*-MePhS($\tilde{X}$) radicals are formed with significant vibrational excitation, which subsequently cools on a ~5 ps time scale. The shape of the strongest *p*-MePhS($\tilde{E} \leftarrow \tilde{X}$) band at λ ~310 nm[22,33] is also better seen in this dataset.

Pulsed radiolysis experiments[36] reveal that the *p*-MePhSH cation has a distinct absorption feature centred at 450 nm, with an estimated maximum extinction coefficient of ~1800 M^{-1} cm^{-1},[37] and a lifetime of >100 ns in cyclohexane. No such feature is observed in the present TA spectra at any delay time, indicating that photoionisation does not occur to any significant extent in these experiments.

The TA signal intensity ratio of the *p*-MePhS($\tilde{X}$) radical absorption at 500 nm to the adduct absorption previously noted at ~380 nm is larger with 200 nm excitation,

(*e.g.*, compare the 50 ps TA spectra in Fig. 3(a) and (b)). This suggests that the geminate recombination noted at 267 nm is much less efficient in the case of higher energy excitation. A more quantitative analysis of geminate recombination is presented in Fig. 3(c) and (d). The integrated area of the *p*-MePhS $\tilde{B} \leftarrow \tilde{X}$ absorption band (integrating over its half peak width $500 \leq \lambda_{probe} \leq 550$ nm to account for vibrational cooling) is plotted against the delay time. It is clear that, consistent with the initial observation, the survival probability of the *p*-MePhS radical is ~60% at 200 ps upon 267 nm photolysis, whereas a 70% survival probability can be obtained for 200 nm photolysis. The radical decay kinetics is in good accord with a full time-dependent diffusion recombination model,[22] where r_{xn} and $\langle r_0 \rangle$ are the only adjustable parameters. The former is the reaction radius—the distance between geminate partners where recombination is assumed to occur instantaneously. The latter is the average separation distance of the photofragments. Fitting the experimental data in Fig. 3 (solid lines) returns average ejection lengths of 9.4 and 12.2 Å at 267 and 200 nm photolysis, respectively, and a reaction radius $r_{xn} = 4.2$ Å. (The diffusion coefficients required in this model, D_H and $D_{p\text{-MePhS}}$ in cyclohexane, are estimated to be 7.67×10^{-4} Å^2 fs^{-1}, using D_H in water[38] and scaling for the liquid viscosities *via* the Stokes–Einstein equation, and $D_{p\text{-MePhS}} \sim D_{benzene} = 2.26 \times 10^{-4}$ Å^2 fs^{-1}, which is estimated from $D_{benzene}$ in ethanol[39] scaled by the appropriate liquid viscosity difference).

iii. Solution photodissociation of PhOH

For phenol, we first describe results at 200 nm where, on the basis of prior gas phase studies, we expect prompt O–H bond dissociation. Fig. 4 displays representative TA spectra of 10 mM phenol in cyclohexane. Although cyclohexane itself produces a moderately strong TA signal in the long-wavelength region (due to two-photon ionisation induced by the pump pulse[40–42]), fortunately it does not contribute significantly in the region where ground state phenoxyl radicals absorb.[43–46] Fig. 4 shows, similar to the ultrafast generation of *p*-MePhS radicals from *p*-MePhSH, PhO($\tilde{X}$) radicals are observed within the instrument response time (~180 fs), consistent with direct dissociation on the repulsive $^1\pi\sigma^*$ surface. Moreover, the radicals generated are clearly highly vibrationally excited, signified by the initially broad and structureless band centred at ~390 nm. This observation is also reminiscent to that of *p*-MePhSH upon 200 nm excitation. The contour of the PhO($\tilde{X}$) band contracts

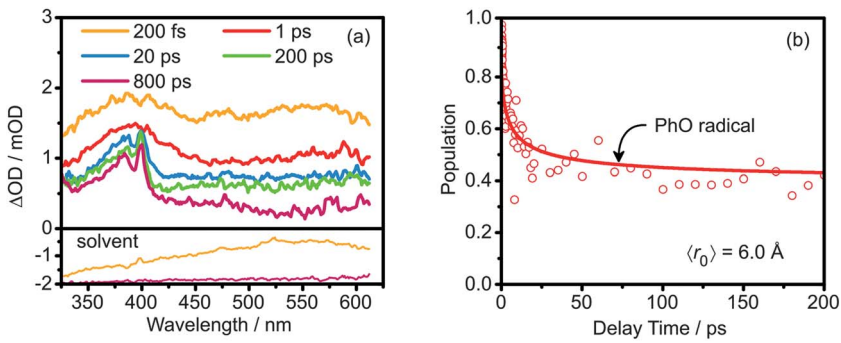

Fig. 4 (a) TA spectra measured at selected time delays following 200 nm excitation of a 10 mM phenol in cyclohexane solution. The TA spectra from the pure cyclohexane solvent, obtained with identical experimental conditions, are shown in the bottom of (a), after subtracting 2 mOD for ease of view. The polarisation of the super continuum probe pulse was set to perpendicular with respect to that of the excitation pulse. (b) Geminate recombination analysis of the radical population after photodissociation (circles) derived from dataset (a). The solid line represents the survival probability, $\Omega(t)$, as predicted by a radical–radical geminate recombination model (see text). From this analysis, $\langle r_0 \rangle = 6.0$ Å.

on a time scale of ~5 ps, thereafter the spectrum of vibrationally "cold" phenoxyl radicals is observed. The latter is known to exhibit a characteristic vibrationally structured absorption band at 380–400 nm,[43–46] with a very similar shape to that observed here. The vibrational relaxation timescale is similar for both PhO and *p*-MePhS radicals; as expected, since this is primarily a function of the solvent.[47]

The decay of the PhO($\tilde{X}$) band is interpreted in terms of geminate recombination with the H atom—an average ejection length of 6 Å can be obtained from the full geminate recombination model (Fig. 4(b)). The constants used in the fitting are identical to those for *p*-MePhSH, with the exception of r_{xn}. The latter is found to be 3.5 Å, obtained from the best fit of the experimental data. Unlike the case of recombination after dissociating *p*-MePhSH, no adduct is observed (at least with an electronic absorption in our spectral window). We note that, as for the thiol system, the data also provide no evidence to support a photoionisation pathway at 200 nm as there is no spectral signature of the phenol cation ($PhOH^+$)—which has an absorption centred at 430 nm and (if it is the final product in the reaction) a life time of hundreds of nanoseconds.[48]

Now we consider the situation where photoexcitation promotes phenol to the S_1 state at energies below the S_1/S_2 CI. The TA spectra of 10 mM phenol in cyclohexane solution following excitation with a 100 fs 267 nm pulse are shown in Fig. 5(a). Within the time window shown, there is no signal attributable to the phenoxyl radical, suggesting no photodissociation. Note that at early time delays a signal due to the cyclohexane solvent also contributes to the total TA, but this makes negligible contribution after 800 ps. The TA spectra before 1 ns are in fact dominated by

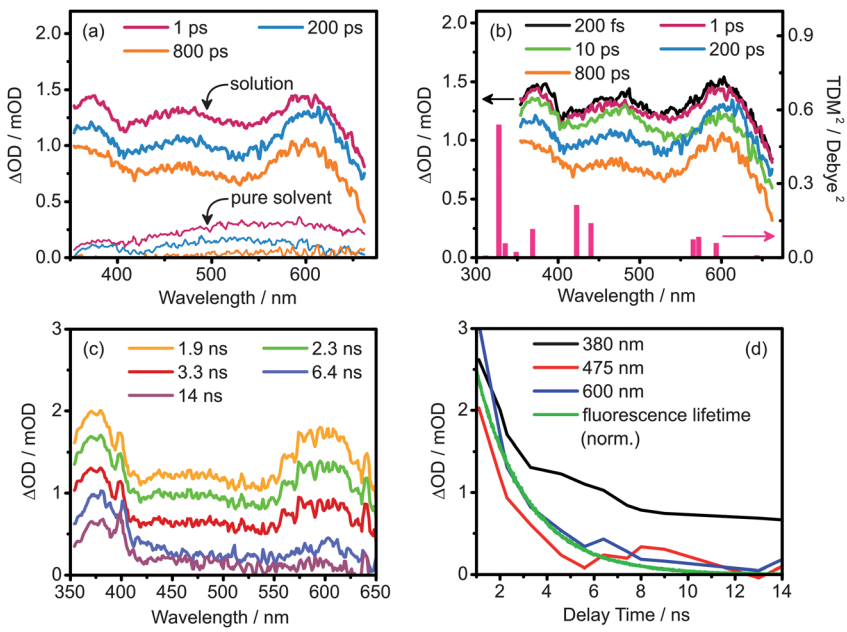

Fig. 5 (a) TA spectra measured at selected delay times following 267 nm photolysis of a 10 mM phenol in cyclohexane solution. The polarisation of the super continuum is set to magic angle with respect to the pump. Thick lines: TA signals from the phenol solution; thin lines: TA signals from pure cyclohexane. (b) TA spectra measured following 267 nm photolysis of 10 mM phenol in cyclohexane, superposed over the calculated squares of the transition dipole moments for excitations originating from S_1. (c) TA spectra measured at nanosecond delay times after 267 nm excitation of 10 mM phenol in cyclohexane. (d) Kinetics at selected wavelengths obtained from the TA experiment and S_1 fluorescence lifetime obtained from TCSPC experiment (green line).

the ESA of the S_1 state, which is populated by absorption of one 267 nm photon. This ESA is evident within our best instrument response time 52 fs (data not shown) and matches well with the calculated $S_n \leftarrow S_1$ EOM-CCSD/aug-cc-pVTZ energies and the square of the TDMs (Fig. 5(b)). Further, it has a similar shape to that obtained by Hermann *et al.*[49] in cyclohexane at 100 ps. The centres of the three major features (at 380, 475 and 600 nm) display identical kinetics, indicating that they originate from the same state.

Although there is no sign of dissociation products within the first nanosecond, we do see the appearance of the phenoxyl radical on longer time scales. Fig. 5(c) presents spectra measured at various delays in the range 1.9–14 ns, which clearly reveal the progressive appearance of the spectral signature of the phenoxyl radical. Fig. 5(d) shows that the kinetics of the 475 and 600 nm ESA bands are consistent with the fluorescence lifetime over the extended time scale (1–14 ns). The 2.1 ns fluorescence lifetime is consistent with that measured by Berlman[50] and by Bent and Hayon.[51] These are further confirmations that the spectral signature observed in 10 mM phenol in cyclohexane at $t < 1$ ns indeed originates from $S_n \leftarrow S_1$ ESA transitions. The kinetics of the 380 nm TA deviate from the S_1 lifetime, however, due to the generation of the PhO radical. The observation of PhO radical absorption is consistent with the earlier flash photolysis study of Hermann *et al.*, but no time scale for the bond fission was reported in that work as a result of the limited available time resolution.[49]

iv. Photoinduced dynamics of PhOH clusters

Both UV-visible[52,53] and IR spectroscopy[54] have demonstrated the possibility of forming phenol clusters in more concentrated cyclohexane solutions (see Fig. 6). As for gas phase clusters,[55] H-bonding between two or more phenol molecules is the main driving force for clustering. We have reproduced the literature results by monitoring the absorption strength of free O–H stretch at 3617 cm^{-1} by FT-IR spectroscopy—the results are shown in the Supplementary Information.† It is estimated from this data that only ~70% of phenol molecules in a 90 mM PhOH in cyclohexane solution exist as isolated monomers, with the remainder present as dimers and higher cluster chains.

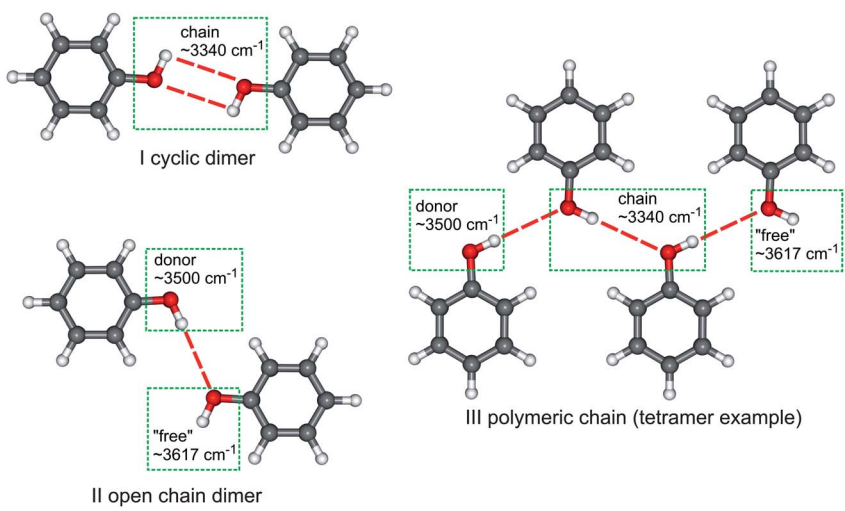

Fig. 6 Illustration of different structures of dimeric and polymeric phenol complexes and the associated OH stretch wavenumbers.

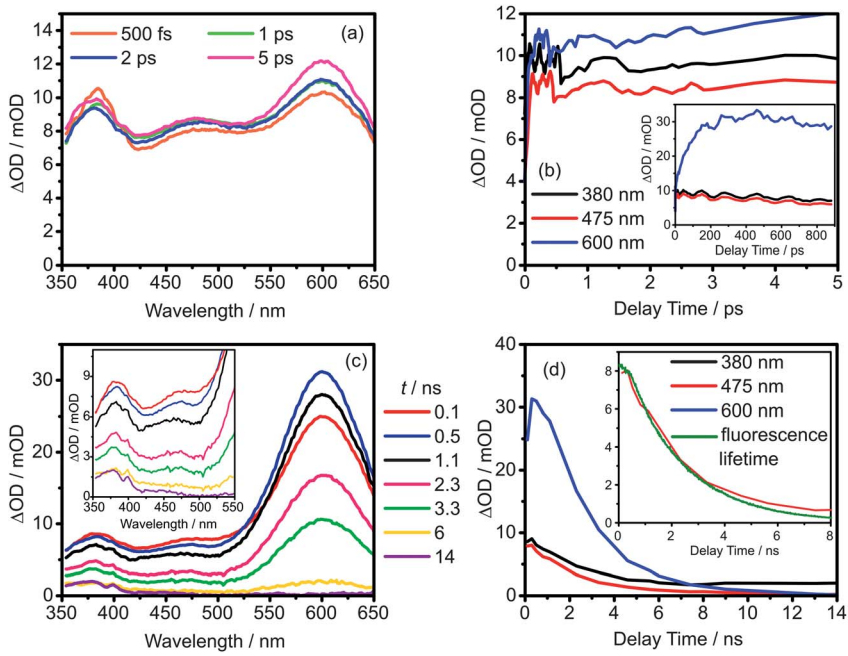

Fig. 7 (a) TA spectra measured at $t < 5$ ps following 267 nm photoexcitation of a 90 mM phenol in cyclohexane solution, with the polarisation of the super continuum probe pulse set to magic angle (54.7°) with respect to that of the excitation pulse. (b) Kinetics of selected wavelengths obtained from the TA experiment at $t < 5$ ps. Inset: $t < 900$ ps. (c) TA spectra measured at delay times in the range 100 ps to 14 ns following 267 nm photexcitation of 90 mM phenol in cyclohexane. Inset: phenoxyl radical region displayed on an expanded scale. (d) Kinetics of selected wavelengths obtained from the TA experiment. Inset: Comparison of the kinetics at 475 nm and the fluorescence lifetime obtained from the TCSPC experiment (same data as shown in Fig. 5(d) but displayed with a different normalization factor).

Fig. 7 presents the result of femtosecond TA experiments following 267 nm excitation of a 90 mM PhOH solution. The transient spectra observed at early delay times ($t < 2$ ps) display three distinct features at 380, 475 and 600 nm, with approximately equal intensities (see Fig. 7(a)), reminiscent to those observed at low concentrations where clustering is relatively much less important. Further, the kinetics of the $\lambda = 475$ nm feature is again in good accord with the 2.1 ns fluorescence lifetime recorded at low phenol concentration (Fig. 7(d) inset). Because these kinetics are identical to those observed in 10 mM phenol solutions, and are consistent with the computed ESA spectrum for the gas phase monomer, we assign these ESA signatures to monomer (or 'monomer-like') S_1 excited phenol. However, the 600 nm peak behaves differently in these high concentration phenol solutions, growing strongly at later times. The original 'monomer-like' 600 nm ESA peak is clearly supplemented by a new transient, such that it ends up with a different set of associated kinetics *cf.* the monomer kinetics at 380 and 475 nm after $t > 2$ ps (see Fig. 7(b) and (d)). The appearance of a new transient, at concentrations where ground state phenol clustering takes off, hints that the new feature may be attributable to phenol excimers. In fact, this broad feature is very similar to the known spectrum of the benzene excimer,[56] where there is an excited state attractive interaction between two stacked π systems. Here, however, the ~100 ps appearance time is much faster than the diffusion limit (*e.g.*, the benzene excimer formation in cyclohexane has a diffusion-limited rate of $(2 \pm 1) \times 10^{10}$ $M^{-1}s^{-1}$[56]). Phenol is different from benzene in that it forms a stable dimer in the ground state, which already places two or more aromatic rings primed in close proximity. Therefore, the rise time seen here represents the

conformational rearrangement of the cluster instead of a diffusional encounter time. We will return to discuss this feature in section IV.

By comparing Fig. 7(a) and (c) we conclude that no appreciable amount of phenoxyl radical is generated within 1 ns, but that a clearly measurable amount is produced on a longer (ns) time scale. These findings are qualitatively consistent with the observations in the 10 mM PhOH solution, but since there is a large error associated with the PhO radical yield measurement it is difficult to determine whether the radical is generated exclusively from the 70% monomer, or if it contains some contribution from the clustered form as well.

We are now poised to explore whether for phenol molecules tied up in clusters, prompt dissociation induced by exciting above the S_1/S_2 CI will turn off dimer conformational rearrangement—thereby eliminating the spectral signature of excimers. Such experiments, using 200 nm excitation, are presented in Fig. 8. We note that Fig. 4, a "control" experiment for this section which should involve negligible clustering, shows no appreciable signal attributable to PhOH S_1 ESA at longer delay times, the signature for which is displayed in Fig. 5. Although we cannot quantify yields accurately, this observation suggests that most monomeric phenol dissociates at 200 nm, or at least that very little undergoes internal conversion to get trapped on S_1.

Due to the large extinction coefficient of phenol at 200 nm, 45 mM phenol solution was used instead of 90 mM to maintain reasonable optical density samples. This diminishes the cluster fraction to ~15%. For the isolated phenol molecules that make up the majority of the solution, vibrationally excited radicals are formed within the instrument response time just as in Fig. 4, indicating direct O–H bond fission as before. Vibrational cooling occurs on a similar timescale to that observed in the low concentration experiment. However, the peak we have assigned to excimer absorption is still observed, suggesting that a significant fraction of the phenol clusters present do not directly dissociate upon 200 nm excitation. Interestingly, an underlying absorption spreading across the whole spectral window is more pronounced compared to the 10 mM solution (*cf.* Fig. 4), probably due to a lesser relative contribution from the solvent TA signal. Single wavelength analysis of 475 nm, where the monomer S_1 ESA exhibits a weak peak (*cf.* Fig. 5) but is otherwise free of contributions from PhO radical and excimer absorption, shows kinetics very similar to that of the 10 mM solution at 267 nm excitation—a single exponential decay which can be best described by a time constant of 2.1 ns. This could imply that those phenol clusters that are unable to dissociate undergo radiationless decay to S_1, where the 'monomer-like' and excimer forms are in equilibrium with the dimer exploring conformational space.

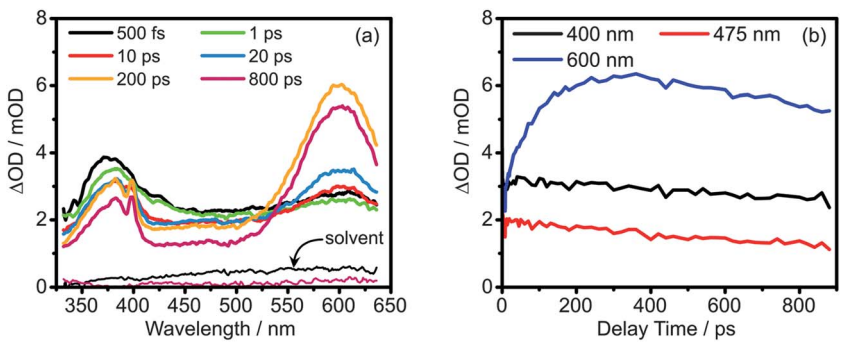

Fig. 8 (a) TA spectra measured at selected time delays following 200 nm photolysis of 45 mM phenol in cyclohexane, with the super continuum probe pulse polarisation aligned parallel to that of the excitation pulse. The thin lines are the TA signal for pure cyclohexane at 500 fs and 800 ps (same colour code as the solution) (b) Kinetics at selected wavelengths.

IV. Discussion

Let us first summarize the major results here in the context of other experimental work. Gas phase photolysis of *p*-MePhSH at wavelengths near 200 nm yield TKER spectra that are consistent with all so far reported,[21,22] in that they indicate formation of $\tilde{X}$ and $\tilde{A}$ state *p*-MePhS radical products. The recoil velocity distribution of the fast H atom products is anisotropic at all wavelengths, implying that dissociation occurs on a timescale faster than that for excited parent molecular rotation.[21,22] When *p*-MePhSH is photoexcited in cyclohexane, at either 267 or 200 nm, a TA attributable to *p*-MePhS($\tilde{X}$) radicals is observed within the instrument response time, confirming H atom loss by prompt S–H bond fission at both wavelengths. The *p*-MePhS($\tilde{X}$) radicals are formed vibrationally excited, most especially at $\lambda_{pump} = 200$ nm, where a broad contour is observed initially and subsequently sharpens within ~5 ps. The translational energy release is reflected in the solution data by the extent of geminate recombination, *i.e.*, by the decay of the *p*-MePhS($\tilde{X}$) TA at 500 nm and the coincident rise of the adduct TA at 380 nm. From the ratio of radical to adduct, it is evident that geminate recombination is less efficient in the case of 200 nm excitation, which suggests a longer H atom ejection length consistent with the greater TKER observed in vacuum.

Excitation of gas phase PhOH at $\lambda > 200$ nm yields predominantly, if not exclusively, PhO($\tilde{X}$) radicals but an additional small yield of PhO($\tilde{B}$) radicals is observed at $\lambda = 193$ nm.[18] Interpreting product recoil anisotropies measured at such short wavelengths is complicated[13,18] but, based on the PESs, we expect PhOH to dissociate promptly at such short wavelengths.[32] This is in marked contrast with the HRA-PTS and time-resolved VMI results at 266 nm and neighbouring wavelengths, which show isotropic product recoil distributions and nanosecond appearance of H atoms.[13,19,20] Consistently, we find that the photochemistry of PhOH in solution is also very different at 'long' and 'short' wavelengths. As in the gas phase,[13,19] 267 nm photoexcitation of PhOH in cyclohexane must excite the former to levels of the S_1 state lying below the S_1/S_2 CI—as shown by the fact that the TA spectrum at early times (t <1 ns) is dominated by S_1 ESA. PhO($\tilde{X}$) radical absorption becomes increasingly apparent at t >1 ns. Conversely, a 200 nm photon excites PhOH well above the S_1/S_2 CI. In this case, PhO($\tilde{X}$) radicals are observed within the 180 fs instrument response time, with significant vibrational excitation, which subsequently relaxes on a time scale of ~5 ps. No new transient absorptions are observed that might be attributed to PhO($\tilde{A}$) or PhO($\tilde{B}$) radicals, at least within our spectral window.

Finally, when PhOH hydrogen-bonded clusters are prepared surrounded by the cyclohexane solvent, a new TA at 600 nm rises in a time scale of ~100 ps which is attributed to the formation of the excimer. While this is an expected aspect of aromatic photochemistry in the condensed phase for excited states with nanosecond lifetimes, we also see the same band when exciting PhOH at 200 nm, suggesting that the direct O–H bond fission pathway is closed for at least some of the clustered species. Further quantification of this last effect would require careful dissociation yield measurements for the monomeric species at low concentration, knowledge of the monomeric and excimeric S_1 ESA molar extinction coefficients and then conversion of the transient spectra into relative populations for each species.

i. Dissociation mechanisms

The $S_2 \leftarrow S_0$ oscillator strength in isolated PhOH is small,[10,19] and there is no evidence supporting a dramatic increase in the solution phase—for example, the absorption cross section at ~240 nm is negligible in cyclohexane (Fig. 1). Therefore, upon 267 nm excitation, the initially populated excited state of phenol is unambiguously S_1, as predicted by *ab initio* calculations, indicated in the steady state absorption spectrum, and clearly observed (both spectrally and kinetically) in our TA

spectrum. The photon energy provided by 267 nm is higher than the $S_{1(v=0)} \leftarrow S_0$ transition energy, but is lower than the location of the S_1/S_2 CI. Intuitively, the deactivation pathways of excited state PhOH in this region include transfer to S_0 *via* internal conversion (IC) or radiative emission, and to T_n *via* intersystem crossing (ISC). Early studies[55,57] suggest that these three channels are responsible for >80% of the excited state deactivation for isolated PhOH molecules, with IC being the major channel. However, O–H bond fission still occurs at energies beneath the S_1/S_2 CI, on a ns timescale, and with a mean TKER of ~5600 cm^{-1} observed in the HRA-PTS experiments.[13]

In light of the large predicted IC yield and slow dissociation time scale, the O–H bond fission process was first (incorrectly) thought to occur *via* coupling at the S_0/S_2 CI after population (by IC) of high vibrational levels of S_0 with substantial O–H stretch character (see Fig.1).[10,13,31,55] This hypothesis has since been reanalyzed and refuted by new experiments (see below), and the present condensed phase experiment provides further evidence for rejecting this mechanism. The current results show a pattern of reactivity in liquid cyclohexane similar to that observed in the gas phase, namely long-lived S_1 and appearance of PhO($\tilde{X}$) radicals but only on a nanosecond timescale. Since the solvent provides an effective "sink" to dissipate excess vibrational energy,[1–4] a highly excited O–H vibration could not survive on S_0 without vibrational energy transfer to adjacent cyclohexane molecules. For example, for dilute methanol in carbon tetrachloride solution where H-bonding is absent, the relaxation time of the O–H($v = 1$) stretch level was determined to be <10 ps.[58] Therefore, the phenoxyl radicals produced on such a nanosecond time scale are unlikely attributable to this ground state dissociation mechanism.

So what accounts for the slow dissociation of phenol? The gas phase data has recently been re-interpreted in terms of H atom tunnelling from the S_1 state under the lower diabats of the S_1/S_2 CI,[19,59] as originally proposed by Sobolewski, Domcke and co-workers.[60] Evidence for this idea comes from HRA-PTS experiments which revealed that the geminate partner of the H atom, the phenoxyl($\tilde{X}^2B_1$) radical, is formed in a very limited subset of the available vibrational state density, predominantly an odd progression of ν_{16a}, the nuclear motion advanced as the coupling mode facilitating the non-radiative $S_1 \rightarrow S_2$ transfer beneath the S_1/S_2 CI.[19] Pino *et al.* measured an S_1 state lifetime of ~2.4 ns using pump–probe ion time of flight measurements[59] and, very recently, Roberts *et al.* have observed the H atom elimination process directly by time-resolved VMI and deduced an appearance time ≥1.2 ns (limited by the maximum delay measurable in their apparatus) for translationally fast H atoms.[20] Both authors appeal to a simple 1D tunnelling model in just the O–H stretch dimension to justify a nanosecond tunnelling lifetime. This tunnelling would only become more significant with a 2D model because of the lower and narrower barrier due to the coupling mode (ν_{16a}) in the branching plane; Dixon *et al.* estimated a 40% greater tunnelling using a 2D wavepacket model compared to the 1D picture.[19]

Roberts *et al.*[20] found that the measured H atom appearance timescale was seemingly invariant as the excitation wavelength was tuned between 275 and 255 nm, and argued that this was strong evidence for a tunnelling mechanism, since IC to S_0 would be expected to show a strong excitation energy dependence on account of the increasing density of vibrational states. Frequency resolved HRA-PTS experiments had previously shown that excited state O–H bond fission occurred irrespective of the initially photoprepared S_1 vibrational state.[13,19,31] The product TKER spectra reveal a marked propensity for S_1 parent vibration to carry through into the phenoxyl radical products—*i.e.* to act as a "spectator" to dissociation. Thus the departing H atom experiences essentially the same tunnelling barrier, irrespective of the particular S_1(v) state excited. However, the parent lifetimes measured by Roberts *et al.* do decrease with increasing photon energy, which is hard to bring into accord with an explanation based on tunnelling in competition with IC. Simple branched kinetics dictates that if parallel processes deactivate the parent, even if

the rate linking parent to product is constant, the appearance time of the product must match the decay of the parent. Thus, while the gas phase ultrafast VMI results provide some support for the tunnelling model, they are not definitive and could also be rationalised with the earlier ground state dissociation mechanism.[13,31]

It appears that the surrounding cyclohexane environment provides little change to the S_1 PES at small O–H bond extensions, which preserves the dynamical behaviour of gas phase PhOH. The dense solvent environment might be expected to push up the Rydberg states of a molecule, however, due to Pauli repulsion of solvent electron density associated with the diffuse solute Rydberg orbital, thereby changing the shape of the S_2 PES—particularly at short $R_{O–H}$ where the Rydberg character is significant. Given such notions, we might expect some possible change in the shape of the tunnelling barrier, but the current experiments suggest that the tunnelling rate cannot be changed substantially from the gas phase otherwise either the S_1 lifetime would be reduced in solution or a vanishingly small phenoxyl radical yield would be difficult to detect.

For gas phase HRA-PTS experiments at $\lambda_{pump} < 248$ nm, the transition to S_2 ($1^1\pi\sigma^*$) state is deduced to gain oscillator strength by intensity borrowing from the S_3 ($2^1\pi\pi^*$) $\leftarrow$ S_0 transition.[19] Thus, the dissociative state can be populated directly and yield H atoms on an ultrafast time scale.[13,31,32] The state that is initially populated at 200 nm is undetermined, due to the high density of states at this excitation energy, but Fig. 2(a) confirms formation of translationally excited PhO products carrying substantial vibrational excitation. In cyclohexane solution, the observation of vibrationally hot PhO($\tilde{X}$) radicals within the instrument response time (<180 fs) following PhOH excitation at 200 nm is similarly consistent with a direct dissociation mechanism, and clearly distinct from the tunnelling mechanism observed when exciting at much longer wavelengths.

The photochemistry of *p*-MePhSH in cyclohexane also shows strong similarities with the gas phase behaviour. Ultrafast S–H bond fission, implied by the anisotropic H atom recoil velocity distributions in the gas phase experiments, is observed directly in the TA experiments in cyclohexane. A 267 nm photon (4.6 eV) likely excites *p*-MePhSH to a region above, or at least very close to, the S_1/S_2 CI (see Fig. 1). The generation of *p*-MePhS radicals within the first 100 fs is not surprising, as they could arise *either* by efficient coupling at the S_1/S_2 CI (by an analogous tunnelling mechanism to that in PhOH but involving a very much smaller barrier) or by direct $S_2 \leftarrow S_0$ excitation since, unlike in phenol, this transition has reasonable oscillator strength.[21,22] Further details on the dissociation behaviour of *p*-MePhSH and related *p*-substituted thiophenols following excitation at energies close to the S_1/S_2 CI will be discussed in ref. 21.

ii. Product energy disposal

At long $R_{X–H}$ (X=O, S) bond extension, the S_2 and S_0 PESs intersect to form the S_2/S_0 CI, which determines the eventual branching between the $\tilde{X}$ and $\tilde{A}$ states of the radical.[61] Out-of-plane motions like ring torsion and the O–H torsion encourage population transfer between the S_2 and S_0 PESs, and encourage formation of $\tilde{A}$ state radicals. Both *p*-MePhS($\tilde{X}$) and *p*-MePhS($\tilde{A}$) radicals are clearly observed in the gas phase.[21,22] Evidence for $\tilde{A}$ state radical formation in cyclohexane solution within the monitored spectral window and out instrument response time is not conclusive at this stage; this will be commented on in a future paper.[24] Calculations at the CASPT2(9/8)/aug-cc-pVTZ level predicted that the $\tilde{D} \leftarrow \tilde{A}$ transition, the strongest *p*-MePhS($\tilde{A}$) transition within our continuum probe, should lie at $\lambda \sim 363$ nm, but with a TDM less than one tenth that of the $\tilde{B} \leftarrow \tilde{X}$ transition at 500 nm.[22] Thus, if the $\tilde{A}/\tilde{X}$ product branching ratio in cyclohexane solution is similar to that in the gas phase, observing clear evidence of *p*-MePhS($\tilde{A}$) radicals is challenging.

Within the spectral range of our continuum probe, the PhO($\tilde{A}$) radical is predicted to have prominent absorption at ~613 ($\tilde{C} \leftarrow \tilde{A}$) and ~400 nm ($\tilde{E} \leftarrow \tilde{A}$);[62] the latter

would essentially overlap with the ground state PhO radical absorption. Further, PhO($\tilde{A}$) radical production is unlikely to be feasible, energetically, at 267 nm (4.65 eV) excitation (see Fig. 1). As mentioned earlier, there is some hint of some flux branching to the PhO($\tilde{A}$) channel in the gas phase but only when $\lambda_{pump} \leq 230$ nm.[18] As in the thiophenols, the $\tilde{A}/\tilde{X}$ product branching ratio is determined by the planarity (or otherwise) of the parent molecule while in the vicinity of the S_2/S_0 CI.[61] The evidence for PhO($\tilde{A}$) radical production in the gas phase is much less clear than in the case of *p*-MePhSH. This can be reconciled by considering the high barrier for the O–H torsion with respect to the ring. As Fig. 1 shows, the O $2p_x$ lone pair orbital aligns parallel with the π electrons of the benzene ring and forms a favourable configuration, with a torsional barrier height of 1215 cm^{-1} in the ground state (4710 cm^{-1} in the S_1 state).[63] This rigid planar geometry ensures that the dissociating flux follows the diabat, encouraging formation of PhO($\tilde{X}$) radicals. In light of this, the failure to observe the PhO($\tilde{A}$) radical in cyclohexane solution is consistent with the gas phase results. However, any excited state radicals formed would likely undergo fast electronic quenching to the ground state *via* the same S_2/S_0 CI. Such processes (see for example the possible $\tilde{A} \rightarrow \tilde{X}$ quenching of the *p*-MePhS radical[22,24]) would be expected to complete within the first 500 fs, and thus be very difficult to observe the excited state radical with the 180 fs instrument response time afforded by the 200 nm pulse.

Unlike $\tilde{A}$ state radicals, where an obvious quenching pathway can be enumerated, PhO($\tilde{B}$) state radicals have no such efficient relaxation pathway (see PES in Fig. 1(a)). Therefore the absence of any new spectral signature in the 200 nm photolysis data, while not conclusive, is supportive of the gas phase observation that this channel remains closed at this photolysis wavelength.[32] Calculations for the absorption bands of PhO($\tilde{B}$) would help strengthen this conclusion.

iii. Translational energy release

After X–H (X=O, S) bond fission, due to the kinematics of both molecular systems, H atoms depart with substantial kinetic energy. Of course, under a collision free environment, this information is preserved and enables detection of the product TKER. In the condensed phase, the high recoil velocity and small size of the H atom means that most can be expected to require several collisions with solvent molecules prior to translational thermalisation within the liquid. This stopping of the ballistically ejected H atoms is expected to be very fast and is not time-resolved in the present experiments, but a measure of the stopping distance (usually called the H atom ejection length) can be determined in the longer timescale diffusive geminate recombination of the radical pair.

In the spherically symmetric limit and under field-free diffusion of the geminate pair,[64,65] the long time survival probability, $\Omega(\infty)$, of the radical pair is a simple function of ejection length (r_0) and an encounter radius to which the two partners must return in order to recombine, namely $\Omega(\infty) = (1 - r_{xn}/r_0)$. The encounter radius r_{xn} is expected to be different for H recombining with PhO or with *p*-MePhS, but for a given radical partner should not vary with photolysis wavelength; the latter simply determines the ejection length *via* how much translational energy the H atom receives. In principle, with two distinct photolysis systems ejecting H atoms into cyclohexane and different photoexcitation energies we should be able to infer the stopping power of cyclohexane to H atoms of several different kinetic energies.[6] We note that, unlike photodissociation reactions producing slower, heavier fragments, we see no evidence for fast cage recombination[7,9] in the time dynamics of the $\tilde{X}$ state PhO or *p*-MePhS radicals.

The radical survival probabilities after S–H bond cleavage of *p*-MePhSH at 267 and 200 nm, and the ejection lengths obtained from a full time-dependent geminate recombination model,[22,64] are in qualitative agreement with the increase in the average TKER determined in the gas phase experiments. The increase in average

TKER from ~8 500 to ~14 000 cm^{-1} determined in the gas phase studies (Fig. 2(a) and Table 1) correlates with an increase in average ejection length from 9.4 to 12.2 Å (Fig. 3), if we assume that the energy partitioning established in the gas phase maps directly into the cyclohexane solution study. Moreover, the kinetics of the *p*-MePhS($\tilde{X}$) radical and the adduct as deduced by single wavelength analysis at 380 nm show a decay and rise commensurate with one another. This indicates that addition of the departing H atom to the ring, or to the sulphur atom so as to reform the parent molecule, is indeed a plausible geminate recombination channel.[24] We cannot say what fraction recombines at the S atom compared to the ring, but the relatively large r_{xn} value we derive could indicate that the ring is a major site for recombination. As can be seen in the fit, the early time kinetics of both features are not described perfectly, because absorption at these probe wavelengths is contaminated by S_1 ESA. Fortunately, the majority of the geminate recombination kinetics is not affected because of the very short S_1 state lifetime of *p*-MePhSH, thus allowing extraction of ejection lengths.

Comparing the H atom ejected from PhOH at 193 and 206 nm, where we expect an average TKER ~12 000 cm^{-1} (see Fig. 2(b) and Table 1), the geminate recombination observed in cyclohexane appears to be best described by $\langle r_0 \rangle = 6$ Å and $r_{xn} = 3.5$ Å. Note that the deduced reaction radius is larger than the value for H + OH recombination in water (2.7 Å)[66] but, as for *p*-MePhSH, a larger r_{xn} suggests that PhO + H may also recombine at the ring position instead of the O atom. However, in the range of our broadband continuum there is no discernible spectral feature assignable to an H-PhO type adduct—it is possible that the electronic absorption of such species is either too weak, located outside of our probing region, or energetically unfavourable. An ejection length cannot be established from the 267 nm photodissociation, since geminate recombination in this case is faster than the nanosecond generation of the PhO radical itself.

An average ejection length of 6 Å for the H atoms formed by PhOH photolysis at 200 nm appears contradictory, given the ~12 000 cm^{-1} average translational energy release in the photodissociation. In comparison, the deduced H atom ejection lengths from *p*-MePhSH photolysis is ~9 Å (for TKER ~8 500 cm^{-1} at $\lambda = 267$ nm) and ~12 Å (for TKER ~14 000 cm^{-1} and $\lambda = 200$ nm). Let us consider one extreme scenario—namely that the presence of solvent guides all the reactive trajectories along the diabat from *p*-MePhSH(S_2) to ground state radicals (*i.e.*, the branching between *p*-MePhS($\tilde{X}$) and *p*-MePhS($\tilde{A}$) products is dramatically changed)—to see if it could provide a rationale for the apparent contradiction in ejection lengths. Even if we were to further assume that little energy is channelled into product vibrations—a result at odds with the observed narrowing of the product TA narrows with increasing time delay and allow all the reaction exoergicity to be available as product kinetic energy, the $TKER_{max}$ at 267 nm would be 10 000 cm^{-1} (Table 1), still less than the average energy release from PhOH photolysis at 200 nm. As this possibility fails to explain the discrepancy, we revisit one other possibility, that the H atom ejection length from phenol is short because the solvent induces more branching to the PhO $\tilde{A}$ state, an outcome that would substantially lower the initial average TKER. Recall that there was some evidence for PhO-d_5($\tilde{A}$) in TKER spectra for 230 nm photolysis.[18] As explained above, for this scenario to be favoured the O–H bond would need to lie out of plane as the dissociating PhOH molecule, surrounded by cyclohexane, approaches the S_2/S_0 CI. One possible scenario is that the S_2 state is prepared with the OH bond out of plane as a result of initial $S_n \rightarrow S_2$ radiationless transition. Any initial driving force toward planarity upon reaching the S_2 state could be sufficient to preserve these out of plane motions in the O–H torsion, which as the O–H bond extends upon dissociation and essentially becomes a free rotor, will remain excited on approaching the S_2/S_0 CI. Arguing against this hypothesis is the absence of any electronic absorption signature of the transient PhO($\tilde{A}$) product—though, if the oscillator strengths of the *p*-MePhS radical absorptions are any guide, visible transitions involving the $\tilde{A}$ state might be

much weaker than those from the $\tilde{X}$ state.[22] Additionally, we have commented that quenching of the PhO($\tilde{A}$) radical may take place faster that the instrument response. At present, we should treat this as an interesting speculation that could possibly account for the deduced shorter H atom ejection length in phenol. However, we note that the assumptions inherent to the geminate recombination analysis are likely too simplistic when one considers (i) the distribution of H atom kinetic energies, that do not necessarily lead to a Gaussian initial radical distribution as assumed in the diffusive model, and (ii) that these molecular systems do not satisfy spherical symmetry. A full molecular dynamics (MD) simulation that includes the initial ballistic energy release would be required for a more complete investigation.[9]

The kinetic energy dependence of the H atom ejection length from *p*-MePhSH photolysis can be compared to that observed for the Cl and OH radicals produced by photolysis of aqueous HOCl. For this photoreaction, the majority of the excess energy after O–Cl bond fission is released as product translation, and very little O–H vibration is observed.[5,68–70] Madsen *et al.* have further established that the ejection length (r_{Cl-OH}), which ranges from 4.4 to 6.0 Å, scales linearly with initial translational energy over the range 1.6–2.8 eV (12 900–22 600 cm^{-1}).[6] This result is partially supported by MD simulations. The ejection length would be expected to be a linear function of kinetic energy if the friction, in this case from water as the environment, is velocity independent. The present results suggest that cyclohexane is much less efficient at stopping an H atom than water is in arresting heavier radicals.

iv. Excited state dynamics in phenol clusters

In phenol dimers, hydrogen-bonding is the dominant ground state interaction. Upon excitation to the S_1 state, however, π–π interactions become much stronger, and consequentially the aromatic rings move into closer proximity with each other and become aligned in a pseudo-parallel configuration.[71] The precise geometry of the excimer is determined by competing H-bonding and π-stacking interactions, as previously illustrated by rotationally resolved electronic spectroscopy.[67,72,73] The rise in the 600 nm kinetics in our 267 nm data is attributed to such conformational changes of dimeric and polymeric phenol upon excitation.

The effect of H-bonding on the $1^1\pi\sigma^*$ state and potential photodissociation has not been demonstrated in previous condensed phase studies. Intuitively, the collinear O–H···O geometry for the H-bonded phenol dimer should significantly change the electronic structure of the $1^1\pi\sigma^*$ state at larger R_{O-H} distances—becoming bound rather than repulsive. Such a situation has been described by Chipman for the excited state of the water dimer.[74] Consistent with this intuition, considering the observation of the excimer band at 600 nm, the spectra of 45 mM phenol obtained at $\lambda_{pump} = 200$ nm provide tentative evidence that at least some of the clusters do not dissociate upon photoexcitation. This 600 nm band would not appear if all photoexcited phenol molecules dissociated.

Although there have been numerous gas phase phenol dimer spectroscopy studies, the majority have focused on the S_1 state. The key observation is that the S_1 state of the phenol dimer has a notably extended lifetime (16 ns, *cf.* 2.1 ns for phenol monomer).[55] This has been ascribed to elimination of the otherwise important IC channel back to S_0 as the H-bonding between the two phenol molecules lowers the vibrational frequency of the O–H stretch, and in turn makes the latter a less efficient acceptor mode.[55] Such an argument implies that the electronic excitation is localised on the H-bond donor phenol which is consistent with theoretical calculations on the dimer.[67] The excited state lifetime is similarly extended in gas phase phenol/water dimers,[55,75,76] where the phenol O–H bond also acts as the H-bond donor.[76] However, the possible effects of clustering on the tunnelling dissociation under the S_1/S_2 CI on the excited state lifetime were not considered, and this process should be strongly affected. In fact, Brause suggested that in the dimer, the donor O–H bond length is shorter in S_1 compared to monomeric phenol[67] which would result

in making the tunnelling barrier higher and wider (see Fig. 1(a)). As mentioned earlier, the fact that the $1^1\pi\sigma^*$ surface may become bounded at longer R_{O-H} will further impact the likelihood of dissociation.[74] Combined, this suggests that tunnelling dissociation will be a less competitive non-radiative relaxation pathway in the dimer in comparison to the monomer. In our experimental TA data, it is difficult to quantify a reduced phenoxyl yield because of the coexistence of monomer and clustered species in the solutions; the latter being a minor component. However, it is clear that the excimer absorption band at 600 nm has a lifetime longer than 2.1 ns (see Fig. 7). Additionally, the monomer S_1 absorption at 475 nm can be fitted with a bi-exponential decay function—at $t < 4$ ns, the decay is in excellent agreement with the single exponential exhibited by low concentration phenol ($\tau = 2.1$ ns), but deviates from a mono-exponential decay at longer time delays. Given that the π stacked excimer is in conformational equilibrium with an open excited state dimer structure that has little π stacking, the observation of a longer tail to the "monomer" ESA band could then also be explained.

These preliminary experiments on the photochemistry of hydrogen bonded cluster species within inert environments like cyclohexane demonstrate that this approach could provide a rich new avenue of research in comparing reaction dynamics in the two phases.

V. Conclusions

In this study, direct comparisons of the primary energy disposal and the pathways for X–H bond scission have been made for two related photolysis systems either isolated in vacuum or embedded in a weakly interacting room temperature liquid. With the energy disposal patterns revealed by HRA-PTS in the gas phase, we can interpret time-resolved liquid phase studies with a far greater level of detail. In turn, the solution femtosecond transient absorption studies provide new dynamical insights to mechanistic pathways and question the factors that influence passage through conical intersections. In particular, we find common to both phases ultrafast X–H scission (X=O, S) at short pump wavelengths near 200 nm; this is also true for *p*-MePhSH excitation near the S_1/S_2 CI at 267 nm. Electronic and vibrational branching patterns in the liquid are observed through characteristic bands in broadband transient spectra. These broadly mimic observations from the gas phase TKER spectra, but geminate recombination analysis suggests a smaller average translation energy release to the H atom for PhOH photolysis at 200 nm than expected from the TKER spectra. For PhOH photolysis below the S_2/S_1 CI, PhO radical formation takes place on a much longer (nanosecond) timescale in both solution and gas phase.[12,20] Because a mechanism requiring phenol having first decayed from S_1 to S_0 to remain vibrationally excited while progressing towards the S_2/S_0 CI is rather unlikely in cyclohexane, a liquid that encourages efficient (sub-nanosecond) vibrational energy relaxation, this latter observation provides new evidence against a ground state dissociation mechanism for phenol near the S_1 origin and lends further support to a tunnelling dissociation mechanism.

The use of cyclohexane as medium makes possible the measurement of excited state reaction dynamics of hydrogen bonded clusters within a liquid environment that can be explicitly compared with gas phase clusters. Our current experiments give tantalizing evidence for the shutdown of the ballistic scission of the PhO–H bond on S_2 when the excited state phenol acts as hydrogen-bond donor. This is fertile ground for dynamical simulations and new experiments that aim to explore the full nature of the solvent influence in guiding chemical dynamics.

Acknowledgements

We thank Richard Dixon for useful discussions regarding tunnelling dynamics in phenol, Mike Nix and Graeme King for help in collecting the phenol HRA-PTS

spectra, and Saptaparna Das and Anirban Roy for help in collecting the phenol TCSPC data. The work at USC is supported by the US National Science Foundation under CHE-0957869 and at Bristol by EPSRC *via* a Programme Grant (EP/G00224X).

References and notes

1 C. G. Elles and F. F. Crim, *Annu. Rev. Phys. Chem.*, 2006, **57**, 273–302.
2 C. G. Elles, M. J. Cox and F. F. Crim, *J. Chem. Phys.*, 2004, **120**, 6973–6979.
3 J. Larsen, D. Madsen, J. A. Poulsen, T. D. Poulsen, S. R. Keiding and J. Thogersen, *J. Chem. Phys.*, 2002, **116**, 7997–8005.
4 C. Petersen, N. H. Dahl, S. K. Jensen, J. A. Poulsen, J. Thogersen and S. R. Keiding, *J. Phys. Chem. A*, 2008, **112**, 3339–3344.
5 C. L. Thomsen, D. Madsen, J. A. Poulsen, J. Thogersen, S. J. K. Jensen and S. R. Keiding, *J. Chem. Phys.*, 2001, **115**, 9361–9369.
6 A. Madsen, C. L. Thomsen, J. A. Poulsen, S. J. K. Jensen, J. Thogersen, S. R. Keiding and E. B. Krissinel, *J. Phys. Chem. A*, 2003, **107**, 3606–3611.
7 N. Winter and I. Benjamin, *J. Chem. Phys.*, 2004, **121**, 2253–2263.
8 C. G. Elles, M. J. Cox, G. L. Barnes and F. F. Crim, *J. Phys. Chem. A*, 2004, **108**, 10973–10979.
9 C. A. Rivera, N. Winter, R. V. Harper, I. Benjamin and S. E. Bradforth, *Phys. Chem. Chem. Phys.*, 2011, **13**, 8269–8283.
10 M. N. R. Ashfold, B. Cronin, A. L. Devine, R. N. Dixon and M. G. D. Nix, *Science*, 2006, **312**, 1637–1640.
11 A. L. Sobolewski and W. Domcke, *J. Phys. Chem. A*, 2001, **105**, 9275–9283.
12 M. G. D. Nix, A. L. Devine, B. Cronin and M. N. R. Ashfold, *Phys. Chem. Chem. Phys.*, 2006, **8**, 2610–2618.
13 M. G. D. Nix, A. L. Devine, B. Cronin, R. N. Dixon and M. N. R. Ashfold, *J. Chem. Phys.*, 2006, **125**, 133318.
14 A. L. Devine, M. G. D. Nix, R. N. Dixon and M. N. R. Ashfold, *J. Phys. Chem. A*, 2008, **112**, 9563–9574.
15 M. N. R. Ashfold, G. A. King, D. Murdock, M. G. D. Nix, T. A. A. Oliver and A. G. Sage, *Phys. Chem. Chem. Phys.*, 2010, **12**, 1218–1238.
16 M. N. R. Ashfold, N. H. Nahler, A. J. Orr-Ewing, O. P. J. Vieuxmaire, R. L. Toomes, T. N. Kitsopoulos, I. A. Garcia, D. A. Chestakov, S. M. Wu and D. H. Parker, *Phys. Chem. Chem. Phys.*, 2006, **8**, 26–53.
17 A. G. Sage, M. G. D. Nix and M. N. R. Ashfold, *Chem. Phys.*, 2008, **347**, 300–308.
18 G. A. King, T. A. A. Oliver, M. G. D. Nix and M. N. R. Ashfold, *J. Phys. Chem. A*, 2009, **113**, 7984–7993.
19 R. N. Dixon, T. A. A. Oliver and M. N. R. Ashfold, *J. Chem. Phys.*, 2011, **134**, 194303.
20 G. M. Roberts, A. S. Chatterley, J. D. Young and V. G. Stavros, *J. Phys. Chem. Lett.*, 2012, **3**, 348–352.
21 T. A. A. Oliver, G. A. King, D. P. Tew, R. N. Dixon and M. N. R. Ashfold, *in preparation*.
22 T. A. A. Oliver, Y. Zhang, M. N. R. Ashfold and S. E. Bradforth, *Faraday Discuss.*, 2011, **150**, 439–458.
23 J. S. Lim, I. S. Lim, K. S. Lee, D. S. Ahn, Y. S. Lee and S. K. Kim, *Angew. Chem., Int. Ed.*, 2006, **45**, 6290–6293.
24 Y. Zhang, T. A. A. Oliver, M. N. R. Ashfold and S. E. Bradforth, *in preparation*.
25 A. E. Jailaubekov and S. E. Bradforth, *Appl. Phys. Lett.*, 2005, **87**, 021107.
26 C. A. Rivera, S. E. Bradforth and G. Tempea, *Opt. Express*, 2010, **18**, 18615–18624.
27 C. G. Elles, C. A. Rivera, Y. Zhang, P. A. Pieniazek and S. E. Bradforth, *J. Chem. Phys.*, 2009, **130**, 084501.
28 M. J. Tauber, R. A. Mathies, X. Y. Chen and S. E. Bradforth, *Rev. Sci. Instrum.*, 2003, **74**, 4958–4960.
29 For the *p*-MePhSH S_1 ESA spectrum, $S_n \leftarrow S_1$ transitions with A'' symmetry were only calculated for $E < 3.0$ eV (*i.e.*, up to and including the $14\ ^1A' \leftarrow 2\ ^1A'$ transition) due to the large computational cost. The magnitude of A'' TDMs are low due to the orthogonal orbital overlap of the initial and final orbitals involved in the transitions. Therefore we anticipate these transitions will make only a minor contribution to the total calculated S_1 ESA spectrum.
30 MOLPRO is a package of *ab initio* programs written by H.-J. Werner, P. J. Knowles, F. R. Manby, M. Schütz, P. Celani, G. Knizia, T. Korona, R. Lindh, A. Mitrushenkov, G. Rauhut, T. B. Adler, R. D. Amos, A. Bernhardsson, A. Berning, D. L. Cooper, M. J. O. Deegan, A. J. Dobbyn, F. Eckert, E. Goll, C. Hampel, A. Hesselmann, G. Hetzer, T.

Hrenar, G. Jansen, C. Köppl, Y. Liu, A. W. Lloyd, R. A. Mata, A. J. May, S. J. McNicholas, W. Meyer, M. E. Mura, A. Nicklaß, P. Palmieri, K. Pflüger, R. Pitzer, M. Reiher, T. Shiozaki, H. Stoll, A. J. Stone, R. Tarroni, T. Thorsteinsson, M. Wang and A. Wolf, Cardiff, 2010.
31 M. N. R. Ashfold, A. L. Devine, R. N. Dixon, G. A. King, M. G. D. Nix and T. A. A. Oliver, *Proc. Natl. Acad. Sci. U. S. A.*, 2008, **105**, 12701–12706.
32 A. Iqbal, M. S. Y. Cheung, M. G. D. Nix and V. G. Stavros, *J. Phys. Chem. A*, 2009, **113**, 8157–8163.
33 Y. M. Riyad, S. Naumov, R. Hermann and O. Brede, *Phys. Chem. Chem. Phys.*, 2006, **8**, 1697–1706.
34 D. L. Gerrard and W. F. Maddams, *Spectrochim. Acta, Part A*, 1978, **34**, 1205–1211.
35 D. L. Gerrard and W. F. Maddams, *Spectrochim. Acta, Part A*, 1978, **34**, 1219–1223.
36 R. Hermann, G. R. Dey, S. Naumov and O. Brede, *Phys. Chem. Chem. Phys.*, 2000, **2**, 1213–1220.
37 Value taken from phenol cation in water, see T. N. Das, *J. Phys. Chem. A*, 2005, **109**, 3344–3351.
38 T. Ichino, PhD thesis, University of Notre Dame, 2001.
39 *CRC Handbook of Chemistry and Physics*, 91st edn, Taylor and Francis, 2009.
40 T. Shida and Y. Takemura, *Radiat. Phys. Chem.*, 1983, **21**, 157–166.
41 S. Tagawa, N. Hayashi, Y. Yoshida, M. Washio and Y. Tabata, *Radiat. Phys. Chem.*, 1989, **34**, 503–511.
42 L. D. A. Siebbeles, U. Emmerichs, A. Hummel and H. J. Bakker, *J. Chem. Phys.*, 1997, **107**, 9339–9347.
43 D. Pullin and L. Andrews, *J. Mol. Struct.*, 1982, **95**, 181–185.
44 K. Kesper, F. Diehl, J. G. G. Simon, H. Specht and A. Schweig, *Chem. Phys.*, 1991, **153**, 511–517.
45 T. N. Das, *J. Phys. Chem. A*, 2005, **109**, 3344–3351.
46 X. Y. Chen, D. S. Larsen, S. E. Bradforth and I. H. M. van Stokkum, *J. Phys. Chem. A*, 2011, **115**, 3807–3819.
47 R. M. Stratt and M. Maroncelli, *J. Phys. Chem.*, 1996, **100**, 12981–12996.
48 M. R. Ganapathi, R. Hermann, S. Naumov and O. Brede, *Phys. Chem. Chem. Phys.*, 2000, **2**, 4947–4955.
49 R. Hermann, G. R. Mahalaxmi, T. Jochum, S. Naumov and O. Brede, *J. Phys. Chem. A*, 2002, **106**, 2379–2389.
50 I. B. Berlman, *Handbook of Fluorescence Spectra of Aromatic Molecules*, Academic Press, New York, 1965.
51 D. V. Bent and E. Hayon, *J. Am. Chem. Soc.*, 1975, **97**, 2599–2606.
52 M. Ito, *J. Mol. Spectrosc.*, 1960, **4**, 125–143.
53 M. Ito, *J. Mol. Spectrosc.*, 1960, **4**, 106–124.
54 R. Mecke, *Discuss. Faraday Soc.*, 1950, 161–177.
55 A. Sur and P. M. Johnson, *J. Chem. Phys.*, 1986, **84**, 1206–1209.
56 H. Miyasaka, H. Masuhara and N. Mataga, *J. Phys. Chem.*, 1985, **89**, 1631–1636.
57 E. Pines, D. Huppert and N. Agmon, *J. Chem. Phys.*, 1988, **88**, 5620–5630.
58 E. J. Heilweil, M. P. Casassa, R. R. Cavanagh and J. C. Stephenson, *J. Chem. Phys.*, 1986, **85**, 5004–5018.
59 G. A. Pino, A. N. Oldani, E. Marceca, M. Fujii, S. I. Ishiuchi, M. Miyazaki, M. Broquier, C. Dedonder and C. Jouvet, *J. Chem. Phys.*, 2010, **133**, 124313.
60 A. L. Sobolewski, W. Domcke, C. Dedonder-Lardeux and C. Jouvet, *Phys. Chem. Chem. Phys.*, 2002, **4**, 1093–1100.
61 O. P. J. Vieuxmaire, Z. Lan, A. L. Sobolewski and W. Domcke, *J. Chem. Phys.*, 2008, **129**.
62 J. G. Radziszewski, M. Gil, A. Gorski, J. Spanget-Larsen, J. Waluk and B. J. Mroz, *J. Chem. Phys.*, 2001, **115**, 9733–9738.
63 G. Berden, W. L. Meerts, D. F. Plusquellic, I. Fujita and D. W. Pratt, *J. Chem. Phys.*, 1996, **104**, 3935–3946.
64 J. A. Kloepfer, V. H. Vilchiz, V. A. Lenchenkov, A. C. Germaine and S. E. Bradforth, *J. Chem. Phys.*, 2000, **113**, 6288–6307.
65 E. B. Krissinel and N. Agmon, *J. Comput. Chem.*, 1996, **17**, 1085–1098.
66 C. G. Elles, I. A. Shkrob, R. A. Crowell and S. E. Bradforth, *J. Chem. Phys.*, 2007, **126**, 164503.
67 R. Brause, M. Santa, M. Schmitt and K. Kleinermanns, *ChemPhysChem*, 2007, **8**, 1394–1401.
68 A. J. Bell, P. R. Pardon, C. G. Hickman and J. G. Frey, *J. Chem. Soc., Faraday Trans.*, 1990, **86**, 3831–3836.
69 C. G. Hickman, A. Brickell and J. G. Frey, *Chem. Phys. Lett.*, 1991, **185**, 101–104.
70 C. G. Hickman, N. Shaw, M. J. Crawford, A. J. Bell and J. G. Frey, *J. Chem. Soc., Faraday Trans.*, 1993, **89**, 1623–1630.

71 A. Weichert, C. Riehn and B. Brutschy, *J. Phys. Chem. A*, 2001, **105**, 5679–5691.
72 M. Schmitt, M. Boehm, C. Ratzer, D. Kruegler, K. Kleinermanns, I. Kalkman, G. Berden and W. L. Meerts, *ChemPhysChem*, 2006, **7**, 1241–1249.
73 M. Kolar and P. Hobza, *J. Phys. Chem. A*, 2007, **111**, 5851–5854.
74 D. M. Chipman, *J. Chem. Phys.*, 2006, **124**, 044305.
75 R. J. Lipert, G. Bermudez and S. D. Colson, *J. Phys. Chem.*, 1988, **92**, 3801–3805.
76 G. Berden, W. L. Meerts, M. Schmitt and K. Kleinermanns, *J. Chem. Phys.*, 1996, **104**, 972–982.
77 The $2^1\pi\sigma^*$ and $2^1\pi\pi^*$ PECs in PhOH (Fig. 1(a)) are adapted from identical calculations where the ring geometry was fixed at the S_0 minimum energy geometry (ref. 19). Here we have shifted the $2^1\pi\sigma^*$ PEC so that it corresponds to the optimized minimum energy of the H + PhO($^2A_2$) products at large R_{O-H} and to the *ab initio* $2^1\pi\sigma^* \leftarrow S_0$ excitation energy in the vFC region (ref. 19). The $2^1\pi\sigma^*$ PEC for *p*-MePhSH (Fig. 1(b)) is far more empirical and based on shifting the $1^1\pi\sigma^*$ relaxed PEC (as shown in Fig. 1(b)) to match the calculated H + *p*-MePhS($^2A_2$) product limit at large R_{S-H} (ref. 22). We have also added a slight "shelf" to this PEC in the vFC region, as we anticipate there will be low-lying Rydberg states with which it will form avoided crossings with this PES.